

# A 3-DOF MEMS MOTION STAGE FOR SCANNING TUNNELING MICROSCOPY

Taekyung Kim<sup>1,2</sup> and Jason J. Gorman<sup>1,\*</sup>

<sup>1</sup>National Institute of Standards and Technology, USA

<sup>2</sup>Erik Jonsson School of Engineering and Computer Science, The University of Texas at Dallas, USA

## ABSTRACT

Piezoelectric tube scanners used in most conventional scanning tunneling microscopes (STM) are highly resonant mechanisms that require a low-bandwidth controller ( $< 1$  kHz) to minimize ringing, which prohibitively limits scan speed. In addition, hysteresis and creep can dramatically limit positioning precision. We report on a microelectromechanical (MEMS)-based three degree-of-freedom (3-DOF) nanopositioner that can replace piezoelectric tube scanners for STM. The presented MEMS nanopositioner has fundamental resonance frequencies of 8.4 kHz in the Z-axis, 27.0 kHz in the Y-axis, and 79.0 kHz in the X-axis, and has sufficient motion range along all three axes for STM operation. This device will enable high-speed atomic-scale imaging and patterning and can be used for parallel STM operation, with multiple integrated tips on a single chip, to increase imaging throughput.

## KEYWORDS

Scanning tunneling microscopy, electrostatic actuator, 3-DOF nanopositioner, motion stage, integrated tip.

## INTRODUCTION

Due to its unprecedented resolution, scanning tunneling microscopy (STM) has been a critical tool for understanding the atomic world since its first invention by Binnig and Rohrer [1]. STM can image surfaces with atomic resolution, revealing individual atoms, and map their local electronic properties. More recently, there has been considerable interest in developing atomic-resolution lithography using hydrogen depassivation, which has been used to pattern atomic-scale devices, such as atomic memories [2], single-atom transistors [3], and individual spin qubits [4].

The piezoelectric tube scanners used in most STMs have a fundamental resonance frequency below a few kilohertz, which sets a strict limit on the scanning bandwidth in order to minimize ringing. In addition, these scanners have both hysteresis and creep, which limit positioning precision. Therefore, while STM can achieve incredible image resolution, it is a very slow measurement process, which has hampered its widespread adoption beyond surface science and has been particularly problematic for tip-based lithography methods.

A number of microelectromechanical scanners have been developed for STM, including a piezoelectric cantilever [5], an electrostatic torsional actuator [6], thermal bimorph actuators [7], and an electrostatic comb actuator [8]. However, a scanner solution has yet to be developed that: 1) works along all three axes,  $X$ ,  $Y$  and  $Z$ , 2) has no motion hysteresis or creep, 3) has high scanning bandwidth, and 4) has an integrated tip for tunneling. Here, we present the design of a MEMS motion stage that is designed specifically for STM and meets the above criteria.

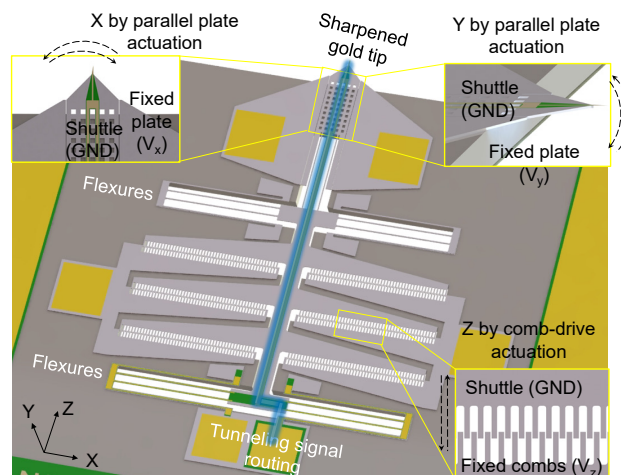


Figure 1: Design of the 3-DOF MEMS nanopositioner with an integrated tip for scanning tunneling microscopy. The insets show the actuation mechanisms for each motion axis.

Characterization results for both the quasi-static and dynamic motion of the stage are described, showing that it has high scanning bandwidth and sufficient scan range for most applications of STM.

## DESIGN AND FABRICATION

A schematic illustration of the 3-DOF MEMS nanopositioner is shown in Fig. 1. The device has a center shuttle suspended by two sets of folded flexures that exhibit a large linear deflection range for the Z axis. An electrostatic comb actuator is used to move the Z axis with a range of approximately  $6 \mu\text{m}$ . This relatively large range was selected to aid in the process of engaging the STM probe with a sample, which could be challenging for multi-tip STM arrays without sufficient range to compensate for angular offsets and microfabrication tolerances. Electrostatic parallel-plate actuators are used for the X and Y axes since they provide sufficient range for scanning; STM typically only requires a scan area around  $100 \text{ nm}^2$ . The X-axis actuator uses an electrode in the plane of the chip to generate an electrostatic force, whereas the Y-axis actuator uses the silicon-on-insulator (SOI) handle wafer as an electrode. This stage design was optimized for high-speed scanning, where the X and Y axes are independent of the Z-axis motion.

There is a metal tip at the end of the shuttle that is electrically isolated from the actuators using a dielectric layer. The tip is sharpened by focused ion beam milling and is made of gold in this case, but can be fabricated from most thin-film metals. By minimizing the footprint of the scanner and having the tip hang over the edge of the chip, multiple scanners can be placed on a single chip for parallel operation in imaging and lithography modes.

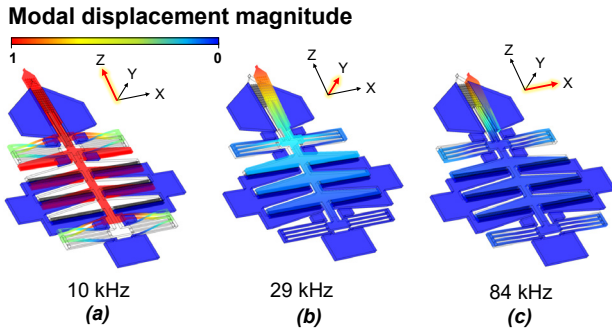


Figure 2: Finite-element analysis for the fundamental modes of each motion axis of the 3-DOF MEMS nanopositioner. (a) Z-axis, (b) Y-axis, and (c) X-axis.

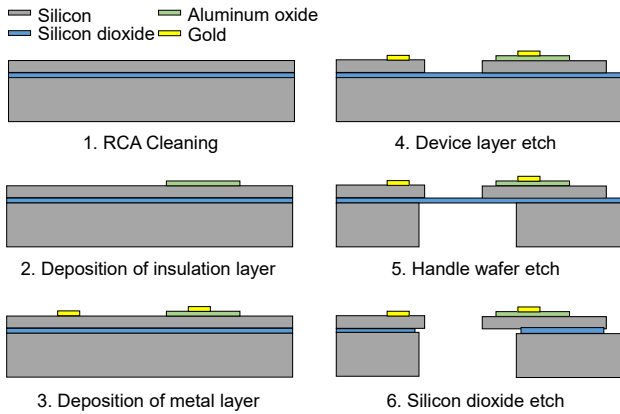


Figure 3: Schematics of the microfabrication process.

### Z-axis stiffness requirements

The Z axis of the MEMS nanopositioner can be modeled as a spring-mass-damper system, where the center shuttle is a lumped mass and the folded flexures are springs. The Z-axis stiffness must be sufficiently large to avoid snap-in due to the attractive electrostatic, van der Waals, and capillary forces at the tip-sample interface. The stiffness requirement is a function of the tip and sample materials, tip radius, bias voltage, and tip-sample distance [8]. Our initial tunneling experiments will use a gold tip with a radius of approximately 30 nm, a highly-oriented pyrolytic graphite (HOPG) sample, a separation distance of approximately 0.5 nm in air, and a bias voltage of 3 V. In this case, the stiffness must be greater than 83 N/m, which was used to set the dimensions of the folded flexures.

### Mode shapes

The folded flexures provide higher stiffness along the X and Y axes compared to the Z axis. This makes it possible to separate the fundamental modes for the actuators in the X and Y axes from the first resonance mode of the Z axis. Modal analysis of the motion stage was performed using finite-element analysis software, where the resulting natural frequencies and mode shapes are presented in Fig. 2. The modal analysis shows that the first resonance for the Z axis is around 10 kHz and the motion is purely in the plane of the chip. The fundamental resonance frequencies for the X and Y axes are 84 kHz and 29 kHz, respectively, and the motion is the result of flexural bending of the cantilever located at the end of the center shuttle.

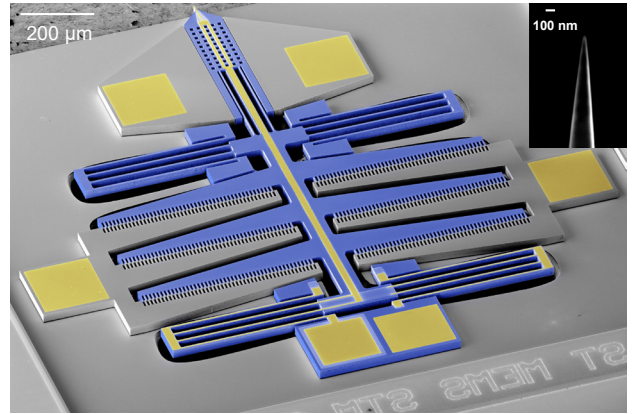


Figure 4: False color scanning electron micrograph of the 3-DOF MEMS nanopositioner with integrated tip. Inset shows the gold tip sharpened by focused ion beam milling.

### Microfabrication

The wafer selected for the fabrication process had a 25  $\mu\text{m}$  thick silicon device layer for the nanopositioner mechanism, a 450  $\mu\text{m}$  thick silicon handle layer, and a 2  $\mu\text{m}$  thick buried oxide layer between the silicon layers. The fabrication of the device followed standard SOI-MEMS processes with the addition of an insulation layer on top of the silicon device layer to isolate the tunneling current signal from the electrostatic actuators, as shown in Fig. 3. We used sputtered aluminum oxide ( $\text{Al}_2\text{O}_3$ ) for the insulating layer, which was deposited after RCA cleaning of a highly doped SOI wafer ( $\approx (0.01 \text{ to } 0.02) \Omega\text{-cm}$ ) and the layer was patterned using a lift-off process. Subsequently, the metal layer was deposited and the device layer etched using deep reactive ion etching (DRIE). The handle wafer was etched by DRIE, and finally, after singulation, the device was released with a vapor HF process. A representative fabricated nanopositioner is shown in Fig. 4.

### STM tip sharpening

The sharpness and conductivity of the tip are crucial for the resolution and reliability of STM measurements. By integrating a tip into the motion stage, devices with more repeatable geometry can be attained compared to assembly or tip deposition. Focused ion beam (FIB) milling was used to shape the metal layer at the end of the center shuttle into a sharp tip, as shown in the inset of Fig. 4. A nominal ion beam current of 7.7 pA at an acceleration voltage of 30 kV was used for the milling. The measured tip radius was about 30 nm and the measured resistance between the tip and the connected bond pad was approximately 50  $\Omega$ , indicating that additional impedance was not added by the milling process. Importantly, it was found that the milling process did not cause electrical shorts in the electrostatic actuators due to material redeposition during milling.

### CHARACTERIZATION

Following fabrication, the device was wire bonded to a ceramic dual-in-line package for characterization. Here, we focused on measurements of the quasi-static motion and the motion frequency response of the three axes, which are important characteristics for comparison with piezoelectric tube scanners.

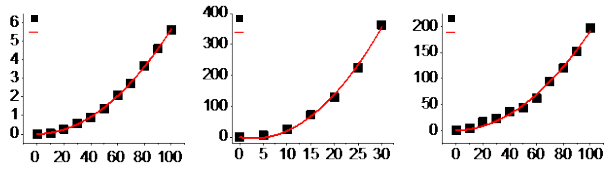


Figure 5: Measured quasi-static displacement as a function of actuation voltage for the (a) Z-axis, (b) Y-axis, and (c) X-axis. The displacement standard deviation at each voltage is smaller than the square marker.

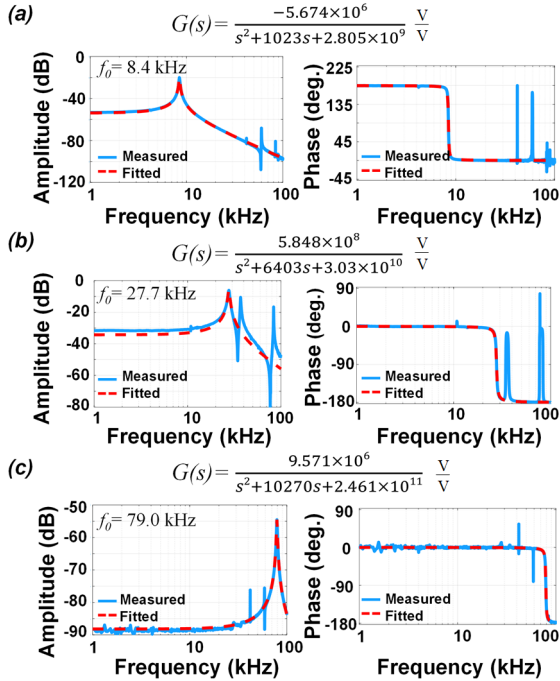


Figure 6: Measured frequency responses. The optical knife-edge method was used for the Z-axis (a) and X-axis (c), and a homodyne interferometer was used for the Y-axis (b). A second-order harmonic oscillator model, where  $G(s)$  is the Laplace transform for this model, was fit to each data set.

### Quasi-static response

The relationship between displacement and actuation voltage is shown in Fig. 5 for all three axes. Three measurement methods were used to characterize the quasi-static displacement response of the three axes; optical microscopy for the Z axis, white light interferometry for the Y axis, and scanning electron microscopy for the X axis. The motion stage was found to have a range of 200 nm, 400 nm, and 6  $\mu\text{m}$  for the X, Y, and Z axes, respectively, when driven with a voltage at or below 100 V. The scanning range in the X-Y plane is more than sufficient for STM.

### Frequency response

The frequency responses for the Z and X axes were measured using the optical knife-edge method [9] from 1 kHz to 100 kHz. The frequency response for the Y axis was measured with a homodyne interferometer. A 2.5 V bias was applied to the actuator and the laser beam was centered on a moving edge. Using the swept-sine method on a dynamic signal analyzer, the frequency response was then measured. The measured resonance frequencies match

well with the finite-element analysis (measured =  $(8.4 \pm 0.15)$  kHz,  $(27.7 \pm 1.4)$  kHz,  $(79.0 \pm 03.9)$  kHz; simulated  $\cong 10$  kHz, 29 kHz, 84 kHz). In all cases, the response closely matches with a second-order system model at and below resonance, which will greatly simplify high-speed scanning using simple open-loop control methods.

## CONCLUSION

In this work, we presented the design, fabrication, and characterization of a 3-DOF MEMS nanopositioner with an integrated tip that has been developed to replace piezoelectric tube scanners used in STM. The characterization results show that the nanopositioner has sufficient motion range for STM and there were no signs of hysteresis or creep in the motion, unlike piezoelectric scanners. Dynamic measurements showed that the resonance frequencies are much higher than found in tube scanners, thereby providing greater scanning bandwidth. In addition to high-speed scanning, the small footprint of the presented design provides an opportunity for high-throughput STM using multi-tip parallel operation.

## ACKNOWLEDGEMENTS

This work was supported by the U.S. Department of Energy, Office of Energy Efficiency and Renewable Energy, Award No. DEEE0008322. This research was performed in part in the NIST Center for Nanoscale Science and Engineering Nanofab.

## REFERENCES

- [1] G. Binnig and H. Rohrer, "Scanning tunneling microscopy," *Surf. Sci.*, vol. 126, pp. 236-244, 1983.
- [2] R. Achal et al., "Lithography for robust and editable atomic-scale silicon devices and memories," *Nat. Comm.*, vol. 9, 2778, 2018.
- [3] M. Fuechsle et al., "A single-atom transistor," *Nat. Nanotechnol.*, vol. 7, pp. 242-246, 2012.
- [4] E. Bussmann et al., "Atomic-precision advanced manufacturing for Si quantum computing" *MRS Bulletin*, vol. 46, pp. 607-615, 2021.
- [5] S. Akamine, T.R. Albrecht, M.J. Zdeblick, C.F. Quate, "Microfabricated scanning tunneling microscope," *IEEE Electron Device Lett.*, vol. 10, pp. 490-492, 1989.
- [6] Y. Xu, N.C. MacDonald, S.A. Miller, "Integrated micro-scanning tunneling microscope," *Appl. Phys. Lett.*, vol. 67, pp. 2305-2307, 1995.
- [7] Y. Tang, Y. Zhang, G.K. Fedder, L.R. Carley, "A dual probe STM imaging system and a low noise switched-capacitor transimpedance amplifier," *IEEE Sens. J.*, vol. 13, pp. 2984-2992, 2013.
- [8] A. Alipour, M.B. Coskun, S.O.R. Moheimani, "A MEMS nanopositioner with integrated tip for scanning tunneling microscopy," *J. Microelectromech. Sys.*, vol. 30, pp. 271-280, 2021.
- [9] V. J. Gokhale, J.J. Gorman, "Optical knife-edge displacement measurement with sub-picometer resolution for RF-MEMS," *J. Microelectromech. Sys.*, vol. 27, pp. 910-920, 2018.

## CONTACT

\*Jason Gorman, tel: +1-301-975-3446, gorman@nist.gov